water

MDPI

Article

Slope Stability Evaluation Due to Reservoir Draw-Down Using LEM and Stress-Based FEM along with Mohr–Coulomb Criteria

Binaya Raj Pandey *, Helmut Knoblauch and Gerald Zenz

Institute of Hydraulic Engineering and Water Resources Management (IWB), Graz University of Technology (TU Graz), Stremayrgasse 10/II, 8010 Graz, Austria; helmut.knoblauch@tugraz.at (H.K.); gerald.zenz@tugraz.at (G.Z.)
* Correspondence: binaya.pandey@tugraz.at

Abstract: Rapid Draw-Down (RDD) in an earthfill dam has serious implications for dam safety regarding slope stability issues. The evaluation of reservoir draw-down impact on slope stability was carried out with the Limit Equilibrium Method (LEM) and stress-based Finite Element Method (FEM), using GeoStudio. The time-dependent Factor of Safety (FOS) and nonlinear behavior were evaluated considering 8 h of RDD. The resulting FOS values of 1.28 and 1.27 using LEM and stress-based FEM were classified as unsafe. The minimum allowable draw-down factor of safety value is 1.3, as per the guideline. The suggested two designs, with upstream horizontal filters and increased upstream dam permeability, provided an adequate FOS. However, the nonlinear analysis with coupled FEM has shown that the upstream slope is unstable in all three cases (i.e., as-built design, increased upstream dam shell permeability, and suggested application of horizontal filter layers) considering 8 h of RDD. Several gradual draw-down rates were also tested and it has been found that the FOS increases with decreased draw-down rates. FOS charts, pressure fluctuation, and flow measurements in the upstream dam shell have revealed that slope stability is highly influenced by pore water pressure and draw-down rate. The safe allowable draw-down rate of 20 h was identified, considering the as-built design of the dam.

Keywords: slope stability; Rapid Draw-Down; permeability; pore water pressure; factor of safety; nonlinear behavior

check for updates

Citation: Pandey, B.R.; Knoblauch, H.; Zenz, G. Slope Stability Evaluation Due to Reservoir Draw-Down Using LEM and Stress-Based FEM along with Mohr–Coulomb Criteria. *Water* **2023**, *15*, 4022. https://doi.org/10.3390/w15224022

Academic Editor: Dan Ma

Received: 31 October 2023
Revised: 16 November 2023
Accepted: 17 November 2023
Published: 20 November 2023

Copyright: © 2023 by the authors. Licensee MDPI, Basel, Switzerland. This article is an open access article distributed under the terms and conditions of the Creative Commons Attribution (CC BY) license (https://creativecommons.org/licenses/by/4.0/).

1. Introduction

The safety of an embankment dam depends upon geotechnical design, operation and maintenance, potential loads, and possible permissible stresses that it withholds during critical situations [1,2]. The steady-state seepage and fluctuation of the seepage path due to sudden changes in water level in the reservoir have an impact on effective stresses and shear strength of the soil materials, influencing slope stability [3,4]. RDD in the reservoir water level can cause a failure of slope [5]. The less permeable soil materials of the dam decrease the drain rate during the draw-down, which has a huge effect on excess pore water pressure. The excess pore water pressure in the dam eventually reduces the resisting force, resulting in a lower safety factor against sliding [6]. A quick reduction of water level and excess pore water pressure in the dam can destabilize the slope, resulting in failure [7].

Duncan [8] has described the state of the art for LEM and stress-based FEM, the evolution of computational technique to perform stress-based FEM for stress–strain distribution in a slope and embankments considering in situ stress–strain behavior. Duncan [8] compared the simulated stress-based FEM deformation results with the field measurement, and the simulated deformation was found to be higher than expected as a result of higher stiffness of the soil in the field than in the laboratory due to aging effects. The author also mentioned that the 2D-FEM overestimates the deformation on a V-shape steep valley wall. In the case of traditional LEM for the range of inter-slice normal and shear forces, LEM

is based on the two-equilibrium factor of safety (FOS) equations. One is based upon the horizontal force, while the other uses the moment equilibrium to determine the FOS [8,9].

Lane and Griffiths [10] used Bishop and Morgenstern LEM and FEM for RDD conditions in an embankment to establish a FOS chart, where the resulting FOS values were found to be more or less similar. Oo et al. [11] applied LEM and FEM to evaluate minimum FOS regarding the stability of the slope due to draw-down and found that the FOS computed with FEM was slightly less than LEM considering stress–strain distribution. Hammouri et al. [12] obtained identical critical slip surfaces and illustrated the difference in the percentage of the minimum FOS considering critical slip circles for LEM and FEM. Azadi [13] compared FOS considering different permeability for the case of RDD and found that FOS increases as a result of higher permeability materials, which is reasonable as higher permeability increases the drain rate. However, the minimum FOS obtained from FEM was a bit lower than LEM, as true stress–strain distributions are hard to establish due to the complexity of soil behavior.

Yelbek Bakhitovich[14] investigated the Chardara dam issues with draw-down rates and different reservoir operation levels to justify correlations, where higher negative correlation was achieved between the pore water pressure and minimum FOS. The author identified that the FOS varies from 0.56 to 2.5, based on the draw-down rate and reservoir operation level. Srivastava [15] demonstrated the influence of permeability on seepage drain rate and slope stability considering different material properties. The slope stability analysis based on spatial variation and the effect of fluctuation in the mean value of permeability for different soil slopes was studied. A significant reduction of FOS was observed for steep slopes with higher permeability parameters.

Gottardi et al. [16] discussed the importance of water content, suction, and its influence on seepage and slope stability. The accurate estimation of the probability of slope failures depends upon the boundary conditions to emphasize the importance of a detailed field study. The appropriate installation of time and frequency domain tensiometers and reflectometer field sensors is necessary for the measurements of matric suction and ground movement in order to increase the accuracy of numerical investigation on slope stability. Bhaskar et al. [17] studied the importance of hydraulic properties on transient seepage behavior during the draw-down and analyzed the pore water pressure effects on FOS with the stability chart. The variation of pore water pressure and FOS was estimated based on hydraulic hysteresis, nonhysteresis, and saturated case. Higher FOS was obtained with the nonhysteresis case than expected, which was concluded to be an unsafe design.

Li et al. [18] applied FEM to study the potential of crack development and internal erosion in earth-fill dams due to rapid changes in reservoir water level. The author emphasized that the formation of a large pore water pressure gradient due to unsteady seepage behaviors causes internal erosion. The equivalent permeability coefficient model results have shown that in the case of cracking at the upstream slope, the pore water pressure gradient accelerated the internal erosion. Alonso Pérez de Agreda et al. [19] mentioned thirty-three cases of upstream slope failure due to RDD, describing the critical case of the San Luis dam in California (1980). The Shira earth-fill dam field observed pore water pressure at different locations and was evaluated under the saturated/unsaturated conditions and simulated with the coupled flow-elastoplastic model, which was found to be consistent.

In this paper, a case study of the Middle Marsyangdi Hydroelectric Power Project (MMHPP) rock-fill dam has been considered to evaluate the failure of the slope due to 8 h of RDD, which was undertaken on October 2012 for reservoir flushing [20]. The coupled model in GeoStudio-Version 23.1 has been applied with a valid academic University license of TU Graz. The presented study attempted to evaluate several FOS methods based on force and moment equilibrium methods to define suitable LEM by performing a correlation matrix. The coupled SEEP/W with SLOPE/W model was implemented for LEM and coupled SEEP/W and SIGMA/W with FEM-Slope-Stability was implemented for stress-based FEM analysis.

The main objectives of the reservoir draw-down case study are:

- To evaluate the approach of LEM and stress-based FEM for defining safe allowable draw-down rates.
- To study the influence of change in permeability of upstream dam shell in the FOS.
- To examine the effect of horizontal upstream filter material in the FOS.
- To evaluate the plastic behaviors on the upstream slope during RDD.

2. Materials and Methods

2.1. Case Study

The Middle Marsyangdi Hydroelectric Power Project (MMHPP) with an installed capacity of 70 MW and annual design generation of 398 GWh is located in the Lamjung district of western Nepal [21]. The project was commissioned on the 14 December 2008 by the Nepal Electricity Authority (NEA) [20]. The peaking run of the river project consists of a combined concrete and rock-fill dam with a live storage capacity of 1.65 million m^3 [21].

The interventions on steep mountainous rivers such as in Nepal have to face a lot of sediment issues, since a huge amount of sediment is transported during flood events, which reduces the storage of the reservoir. Therefore, in October 2012, reservoir flushing was carried out to remove the sediment deposited on the right bank of the reservoir at the upstream side of the dam, as presented in Figure 1.

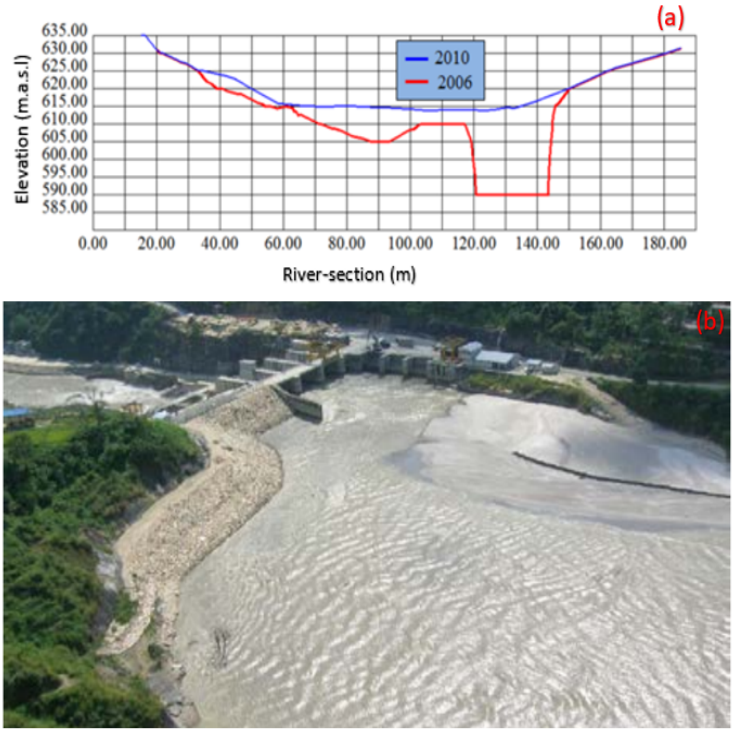

Figure 1. The evolution of the river bed from 2006 to 2010 is represented by (**a**), and (**b**) shows sediment deposition in the MMHPP reservoir at the right bank of headworks [21].

After 8 h of draw-down of the water level in the reservoir for flushing, the slope of the rock fill dam was found to be unstable, and repair maintenance of the rip-rap was carried out to stabilize the slope, as shown in Figure 2. The movement of the boulder rip-rap can be clearly visualized through the reference Figure 2, as a result of excess pore water pressure, even though the design upstream slope of 2.3H:1V was found to be mild.

Figure 2. Instability of the slope after the draw-down is represented by (**a**,**b**) after the draw-down. * represents detail image.

As-built design of the MMHPP rockfill dam consists of a central clay core, vertical coarse and fine filter material, dam shell, and boulder rip-rap to protect the slope, as shown in Figure 3. The dam was designed with a mild slope of 2.3H:1V at the upstream and 2H:1V at the downstream sides concerning the safety against slope instability. The total dam height is 23 m measured from the central axis. The dam has been built on sound impermeable bedrock which prevents flow through seepage, reduces the risk of foundation failure, and prevents excessive settlements.

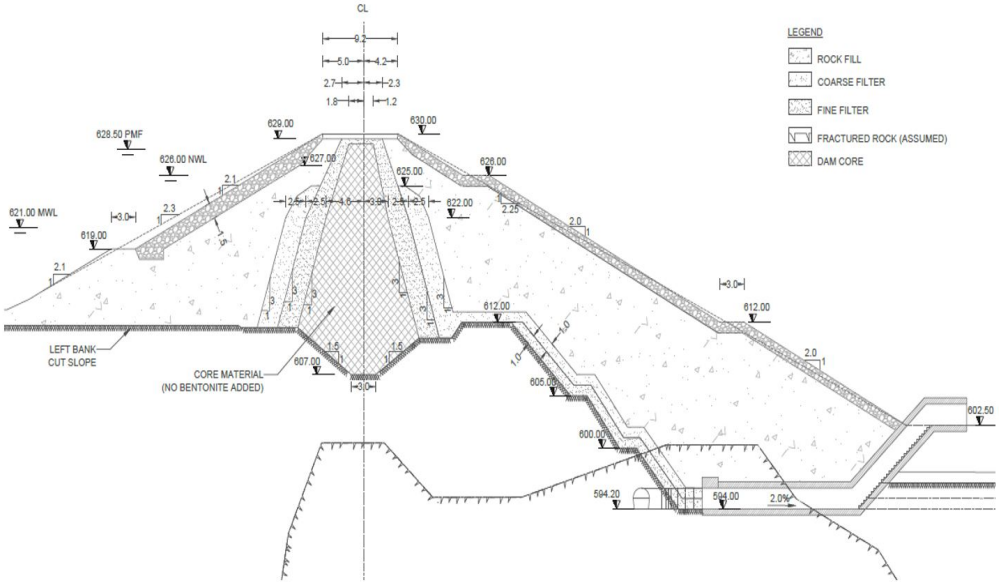

Figure 3. Clay core zonal rockfill dam.

2.2. Material Properties

To understand the seepage flow behavior inside the rock fill dam consisting of various materials, it is essential to define the appropriate soil properties [16]. The materials' properties play a significant role during the design and construction process. The mechanical properties ensure the stability of the dam regarding shear strength, internal erosion, and deformation under various loading conditions. Knowledge of permeability with appropriate drainage filter materials and drainage systems helps to control the seepage enhancing the stability of the dam. MMHPP dam shell consists of a mixture of silty sand, rip-rap consists of boulders, fine filter consists of sand, coarse filter consists of gravel, and clay-core consists of clay. The materials distinguished by the Unified Soil Classification System (USCS) were adopted for parameter values [22].

2.2.1. Soil Water Characteristic Curve (SWCC)

The SWCC describes the change in suction pressure due to the air entrainment causing water to drain out from the soil as a result of negative pore water pressure [23]. The negative pore water pressure changes until it reaches the residual water content, which is considered a fully unsaturated soil condition, as illustrated in Figure 4 [24].

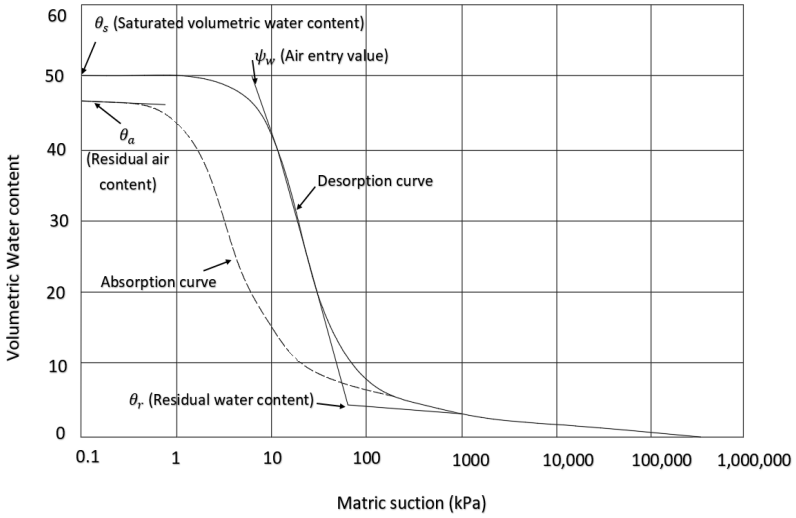

Figure 4. Soil water characteristic curve, Rahardjo [24].

The SWCC for different zonal materials of the dam was adopted based upon the volumetric water content defined by Khire and Bosscher [25] which is presented in Figure 5. The materials distinguished by USCS were adopted, where GP is defined as poorly graded gravel, SP stands for poorly graded sand, SM represents silty sand, ML is defined as silt, and CL represents clay. The sample volumetric water content functions for soil parameters based on the specified saturated and residual water content were used to plot a graph between the volumetric water content and matric suction for different soil materials using SEEP/W [25].

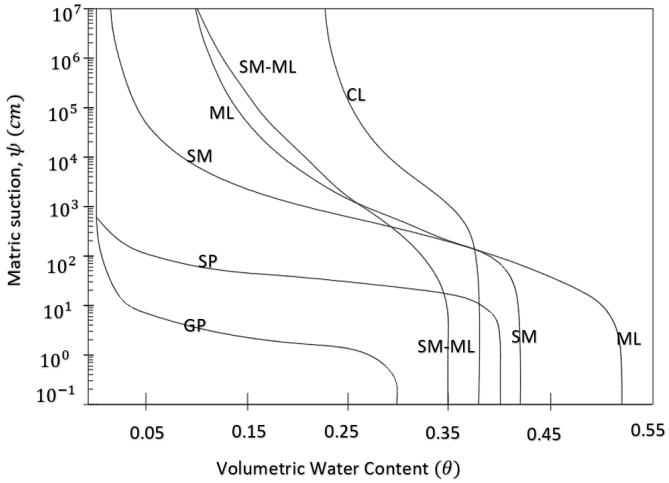

Figure 5. SWCC for different materials defined by Khire and Bosscher [25].

2.2.2. Hydraulic Conductivity/Permeability (k_w)

The conductivity defines a fluid flowing through the porous medium under the influence of a hydraulic gradient, expressed in terms of travel distance per time required on a saturated zone.

Based upon Khire and Bosscher [25] as represented in Figure 6, hydraulic conductivity was adopted for the different materials used in the dam of MMHPP. The hydraulic conductivity (Van Genuchten, 1980) [26] in relation to the suction range was implemented using SEEP/W.

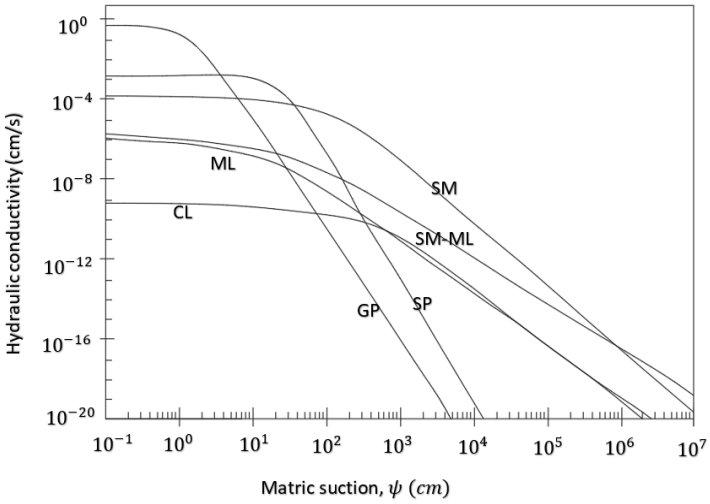

Figure 6. Hydraulic conductivity versus Matric suction, Khire and Bosscher [25].

2.2.3. Angle of Friction (ϕ') and Cohesion (c')

The angle of internal friction characterizes the shear strength of the soil to slide on the failure plane, whereas the cohesive strength of the soil defines the internal bonding or attractive forces between the soil particles, which provides soil materials to retain their shape and resist deformation under loading conditions [24]. The angle of friction and cohesion suggested by Ameratunga [27], as shown in the Table 1 has been used in the model.

Table 1. Cohesion and internal angle of friction, Ameratunga [27].

	Material	ϕ' (°)
Soils	Soft and firm clay of medium to high plasticity, silty clays, loose variable clayey fills, loose sandy silts (use c' = 0–5 kPa)	17–25
	Stiff sandy clays, gravelly clays, compacted clayey sands and sandy silts, compacted clay fill (use c' = 0–10 kPa)	26–32
	Gravelly sands, compacted sands, controlled crushed sandstone, and gravel fill, dense well-graded sands (use c' = 0–5 kPa)	32–37
	Weak weathered rock, controlled fills of roadbase, gravelly and recycled concrete (use c' = 0–25 kPa)	36–43
Rocks	Chalk (c' = 0 kPa)	35
	Weathered granite (c' = 0 kPa)	33
	Fresh basalt (c' = 0 kPa)	37
	Weak sandstone (c' = 0 kPa)	32
	Weak siltstone (c' = 0 kPa)	28
	Weak mudstone (c' = 0 kPa)	32

2.2.4. Modules of Elasticity (E) and Poisson's Ratio (v)

Modules of elasticity help to determine the stiffness of the material; it shows how the material deforms elastically under applied stress and returns to its original position or deforms permanently [28], whereas Poisson's ratio defines the ratio of lateral strain and

longitudinal strain [28]. Figure 7 illustrates the relationship between stress and strain under loading conditions.

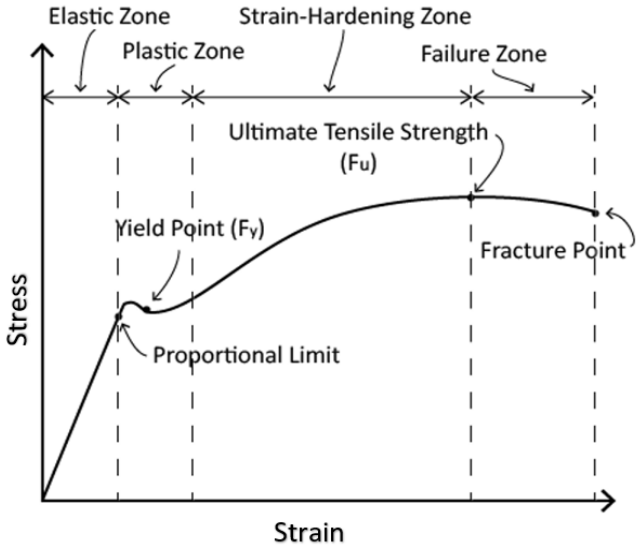

Figure 7. Stress–strain relationship [28].

The Table 2 experimental lab test results defined by the American Association of State Highway and Transportation Officials (AASHTO) [29] were adopted to define the modulus of elasticity and Poisson's ratio of soil materials for the dam.

Table 2. Elastic constants of various soil materials, AASHTO [29].

Soil Type	Typical Range of Young's Modulus (MN/m^2)	Poisson's Ratio
Clay: Soft sensitive	2.4–15	0.4–0.5 undrained
Medium stiff to stiff	15–50	
Very stiff	50–100	
Loess Silt	15–60	0.1–0.3
	2–20	0.3–0.35
Fine Sand: Loose	7.5–10	0.25
Medium Dense	10–20	
Dense	20–25	
Sand: Loose	10–25	0.25–0.35
Medium Dense	25–50	0.3–0.4
Dense	50–75	
Gravel: Loose	25–75	0.2–0.35
Medium Dense	75–100	0.3–0.4
Dense	100–200	

2.3. Governing Equations

2.3.1. Darcy's Law

SEEP/W has been formulated on the basis that the flow of water through the soil follows Darcy's law for the saturated zone [30,31]:

$$q = k \cdot i \quad (1)$$

where
q = specific discharge (m^3/s.m^2);

k = hydraulic conductivity (m/s);
i = gradient of the total hydraulic head.

2.3.2. 2D Partial Differential Flow Water Equation

The governing partial differential equation for two-dimensional seepage implemented in SEEP/W is as follows [32]:

$$\frac{\partial}{\partial x}\left(k_x \frac{\partial H}{dx}\right) + \frac{\partial}{\partial y}\left(k_y \frac{\partial H}{dy}\right) + Q = \frac{\partial \theta}{\partial t} \quad (2)$$

where
H = total head (m);
k_x = hydraulic conductivity in the x-direction (m/s);
k_y = hydraulic conductivity in the y-direction (m/s);
Q = applied boundary flux (m^3/s);
θ = volumetric water content;
t = time (s).

The GeoStudio solver uses the Finite Element Method (FEM) to solve the partial differential equation considering the linear as well as quadratic mesh. For some analyses, such as slope stability and seepage analysis, linear meshes are sufficient to provide accurate results. However, for more complex analyses, such as deformation and stress analysis, quadratic meshes are implemented to capture the curvature and discontinuities of the solution.

2.3.3. Hydraulic Conductivity/Permeability (k_w)

The hydraulic conductivity (Van Genuchten, 1980) [26] in relation to the suction range has been implemented in the model for the unsaturated zone:

$$k_w = k_s \frac{\left[1 - \left(a\psi^{(n-1)}\right)\left(1 + (a\psi^n)^{-m}\right)\right]^2}{\left((1 + a\psi)^n\right)^{\frac{m}{2}}} \quad (3)$$

where
k_w = hydraulic conductivity (m/s);
k_s = saturated hydraulic conductivity (m/s);
a, n, m = curve fitting parameters;
n = express as $1/(1 - m)$;
ψ = required suction range.

2.3.4. Coefficient of Volume Compressibility (m_v)

The coefficient of volume compressibility is expressed as the reciprocal of modules of elasticity often considered equivalent to the coefficient obtained from the 1D consolidation test [28]:

$$m_v = \frac{1}{M} = \frac{a_v}{1 + e_o} \quad (4)$$

where,
M = modulus of elasticity (N/m^2);
a_v = coefficient of compressibility;
e_o = initial void ratio.

2.3.5. Mohr–Coulomb Theory

The shear strength of the soil is defined by the Mohr–Coulomb Equation [28]:

$$\tau = c + (\sigma - u_w)\tan\phi \quad (5)$$

where
σ = stress (N/m^2);
u_w = pore–water pressure (N/m^2);
c (N/m^2) and ϕ (degree) are the intercept on the shear stress axis and the slope of the Mohr–Coulomb failure envelope, as represented in Figure 8.

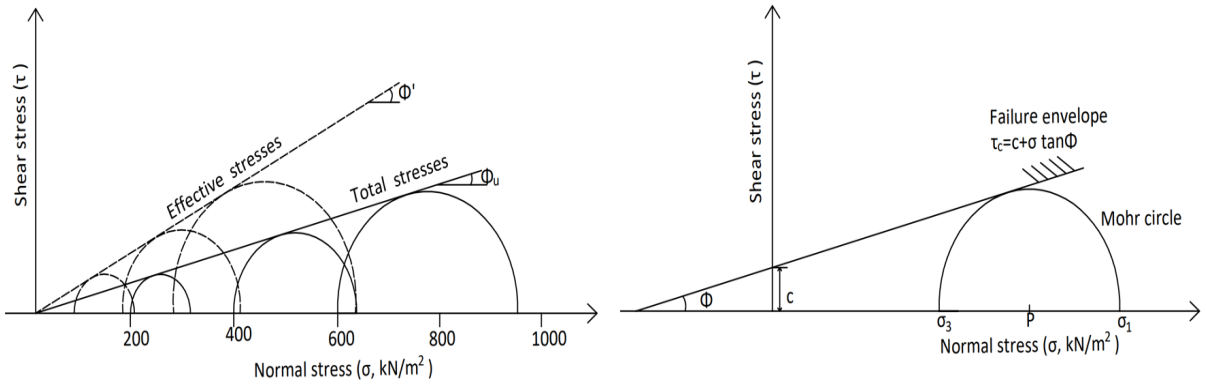

Figure 8. Mohr–Coulomb circle with the failure envelope [28,31].

The Mohr–Coulomb equation is modified to account for suction strength [32]:

$$\tau = c + (\sigma - u_a)\tan\phi + (u_a - u_w)\left[\frac{\theta_w - \theta_r}{\theta_s - \theta_r}\right]\tan\phi \quad (6)$$

where;
u_a = pore-air pressure (N/m^2);
$(u_a - u_w)$ = soil suction (N/m^2);
θ_w = volumetric water content;
θ_r = residual water content;
θ_s = saturated water content.

2.3.6. Methods for Factor of Safety (FOS)

Several methods have been developed to evaluate the factor of safety against sliding over the past years. The difference between the methods depends upon the consideration of inter-slice normal and shear forces and relationships, as well as the force and moment equilibrium method, as illustrated in Table 3 and 4 [32]. The typical forces acting upon the slice are represented in Figure 9.

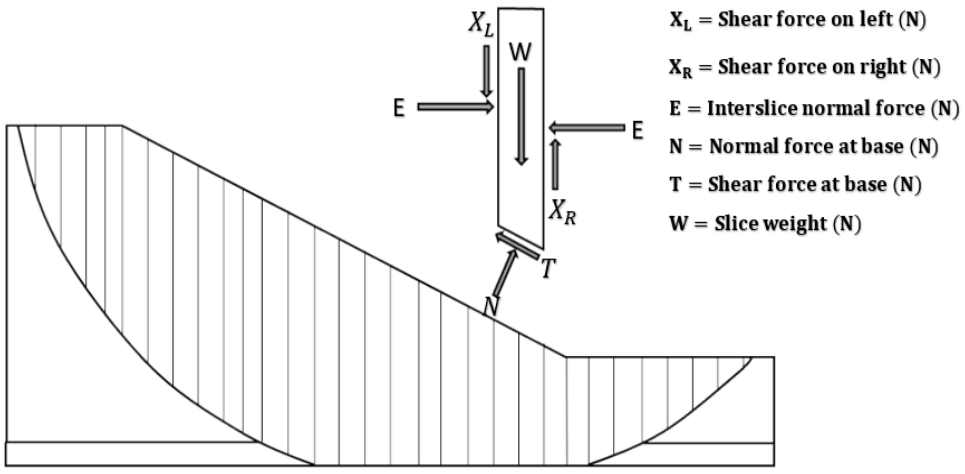

Figure 9. Free body diagram of a slice showing the shear and normal forces (SLOPE/W) [32].

Table 3. Inter-slice force characteristics and relationships (SLOPE/W) [32].

Method	Inter-Slice Normal (E)	Inter-Slice Shear (X)	Inclination of X/E Resultant, and X-E Relationship
Ordinary or Fellenius	No	No	No inter-slice forces
Bishop's Simplified	Yes	No	Horizontal
Janbu's Simplified	Yes	No	Horizontal
Spencer	Yes	Yes	Constant
Morgenstern–Price	Yes	Yes	Variable; user function
Corps of Engineers-1	Yes	Yes	Inclination of a line from crest to
Corps of Engineers-2	Yes	Yes	Inclination of ground surface at top of slice
Lowe-Karafiath	Yes	Yes	Average of ground surface and slice base inclination
Janbu Generalized	Yes	Yes	Applied line of thrust and moment equilibrium of slice
Sarma-vertical slices	Yes	Yes	$X = C + E \tan \phi$

Table 4. Equations of statics satisfied (SLOPE/W) [32].

Method	Moment Equilibrium	Force Equilibrium
Ordinary or Fellenius	Yes	No
Bishop's Simplified	Yes	No
Janbu's Simplified	No	Yes
Spencer	Yes	Yes
Morgenstern–Price	Yes	Yes
Corps of Engineers-1	No	Yes
Corps of Engineers-2	No	Yes
Lowe-Karafiath	No	Yes
Janbu Generalized	Yes (by slice)	Yes
Sarma-vertical slices	Yes	Yes

2.3.7. Limit Equilibrium Method

The general LEM FOS for the horizontal force equilibrium (SLOPE/W) is as follows [32]:

$$F_f = \frac{\sum(c\beta \cos\alpha + (N - u\beta)\tan\phi \cos\alpha)}{\sum N \sin\alpha - \sum D \cos\omega} \quad (7)$$

The general LEM FOS with respect to the moment equilibrium (SLOPE/W) is as follows [32]:

$$F_m = \frac{\sum(c\beta R + (N - u\beta)R\tan\phi)}{\sum Wx - \sum Nf \pm \sum Dd} \quad (8)$$

$$N = \frac{W + (X_R - X_L) - \frac{(c\beta \sin\alpha + u\beta \sin\alpha \tan\phi)}{F}}{\cos\alpha + \frac{\sin\alpha \tan\phi}{F}} \quad (9)$$

where
c = cohesion (N/m^2);
ϕ = angle of friction (degree);
u = pore water pressure (N/m^2);
W = slice weight (N);
D = concentrated point load (N);
β, R, x, f, d, ω = geometric parameters;
α = inclination of slice base (degree).

2.3.8. Stress-Based FEM Method

The normal force at the base of the slice is primarily unknown in a Limit Equilibrium formulation. Plotting the initial in situ stress distribution provides the stress along the slip surface [8]. The stress-based FEM considers the stress–strain distribution within the soil mass considering the soil properties. Therefore, the FOS in each slice is different in

stress-based FEM, whereas the FOS is constant for all the slices along the slip circle in LEM [8].

2.4. Model Parameters

The 2D unstructured meshes consisting of 1995 nodes and 3670 elements were generated, as shown in Figure 10. The used model material properties have been provided in Table 5, as well as presented in Figure 11 and 12.

Table 5. Material properties of different layers.

Materials	k_w (m/s)	Vol. WC	Residual = 10% WC	m_v (kPa^{-1})	Unit Wt (kN/m^3)	Friction Angle (ϕ)	c (kPa)	Modulus of Elasticity (MPa)	Poisson's Ratio
Clay core	1×10^{-8}	0.50	0.05	3.3×10^{-5}	16	25	10	30	0.45
Dam shell	1×10^{-4}	0.40	0.040	2×10^{-5}	20	30	8	50	0.3
Fine filter	1×10^{-3}	0.30	0.030	4×10^{-5}	18	32	2	25	0.25
Coarse filter	1×10^{-2}	0.25	0.025	1.6×10^{-5}	22	35	1	60	0.3
Rip-rap	1×10^{-1}	0.20	0.020	1×10^{-5}	27	37	0.5	95	0.35

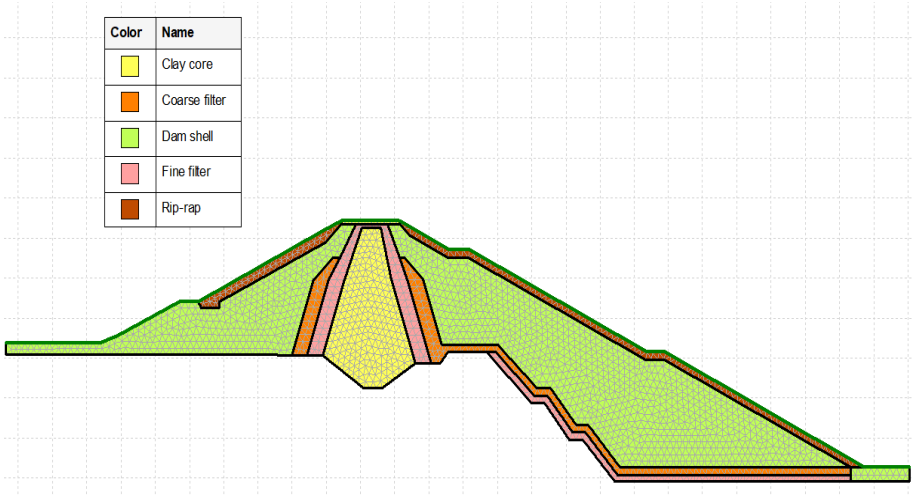

Figure 10. 2D geometry section of the dam.

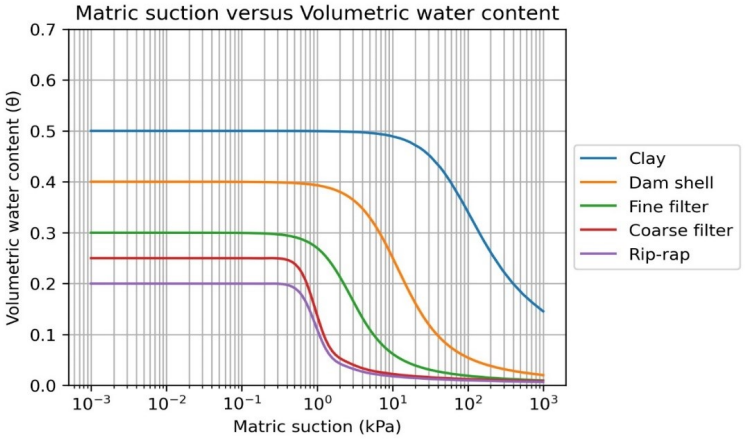

Figure 11. Volumetric water content versus matric suction curve for the unsaturated zone.

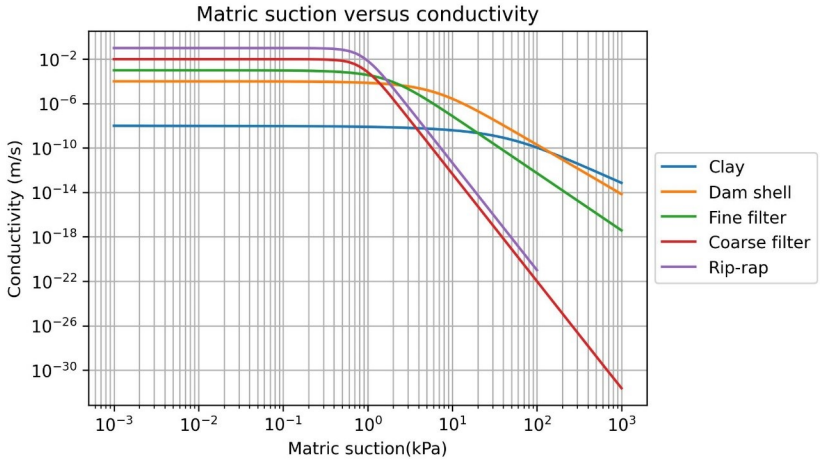

Figure 12. Hydraulic conductivity versus matric suction curve.

2.5. Correlation Matrix

Using a case study of October 2012, a linear draw-down of 8 h for reservoir flushing was considered. The time series of critical FOS was obtained to plot a correlation matrix using various force and moment equilibrium methods for LEM. Morgenstern–Price and Spencer, based on both moment and force equilibrium methods [32], Crops of Engineers#1, Lowe-Karafiath, and Janbu, based on the force equilibrium method [32], and Bishop and Ordinary method, based upon the moment equilibrium [32] are implemented to obtain a correlation matrix.

The Morgenstern–Price, Spencer, Janbu, Bishop, and Ordinary methods were found to be highly correlated, as plotted in Figure 13 with time series of the critical FOS values, which were found to be a tolerance with a third decimal difference. As a result, correlation values were found to be 1 in the case of Morgenstern–Price, Spencer, Janbu, Bishop, and Ordinary methods. The widely used Morgenstern–Price method was adopted for the LEM, which satisfies both the force and moment equilibrium conditions considering inter-slice normal and shear forces, as illustrated in Tables 3 and 4.

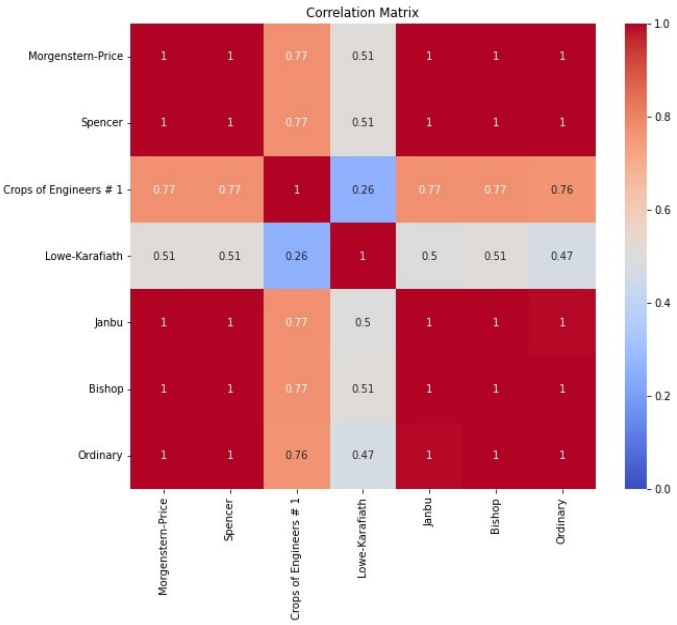

Figure 13. Correlation matrix for different LEM.

3. Results

3.1. Steady-State

The long-term stability analysis considering the as-built design dam was modeled through the steady state to ensure the stability of the dam. A coupled model of SEEP/W and SLOPE/W was carried out to ensure the effect of pore water pressure on the slope stability. The model was coupled with SEEP/W and SLOPE/W for LEM, whereas stress-based FEM was coupled with SEEP/W and SIGMA/W for FEM to analyze the initial state stability of the dam considering the maximum water level in the reservoir. The LEM applied by Morgenstern–Price was adopted to estimate the FOS against sliding at the upstream face of the dam. Conversely, the Finite Element stress method applied with in situ stress was adopted considering the initial stress of the dam. Figures 14 and 15 illustrates the slope stability analyses results defined by critical slip circles, using LEM and stress-based FEM.

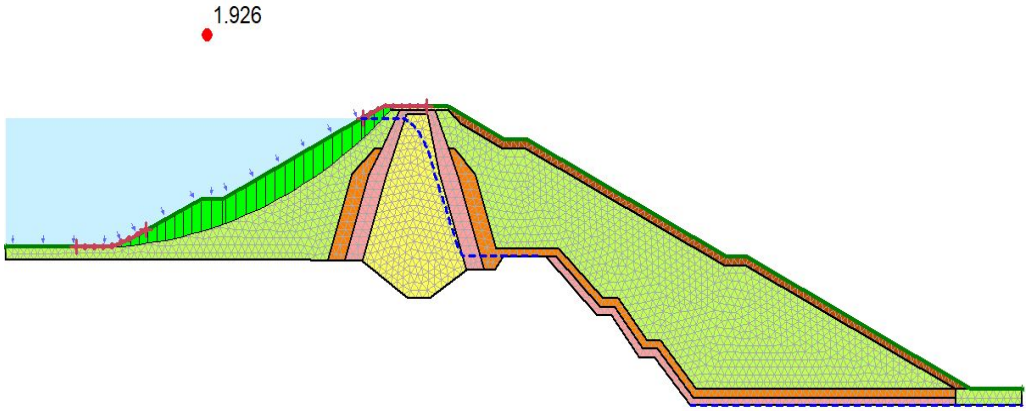

Figure 14. Upstream slope stability analysis using LEM.

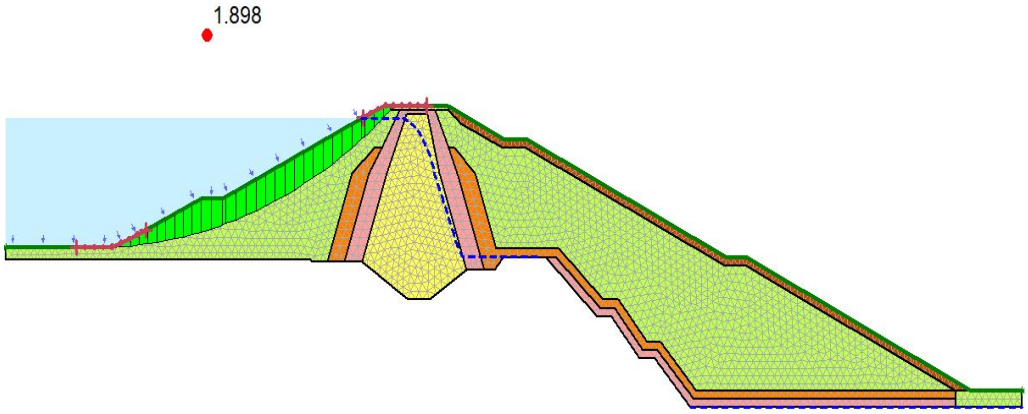

Figure 15. Upstream slope stability analysis using stress-based FEM.

The critical slip circle with FOS value of 1.92 using LEM and 1.89 using stress-based FEM was evaluated at the upstream side of the dam considering the maximum reservoir water level.

3.1.1. Stress Distribution

Normal base stress acting upon the slices was evaluated using LEM and stress-based FEM. Each slice's normal base stresses were plotted considering the equal radius, i.e., 62.4 m of slip circle, as represented by the free body diagram of the slice in Figure 9.

The stress distribution at the base of each slice using LEM and FEM follows more or less the same distribution as illustrated by the results in Figure 16. The stress distribution-based FEM gives more realistic values than the LEM; however, the true stress on the existing

ground may not be the same. It can be concluded that both models match reasonably, exhibiting comparable results and distribution across individual base stress.

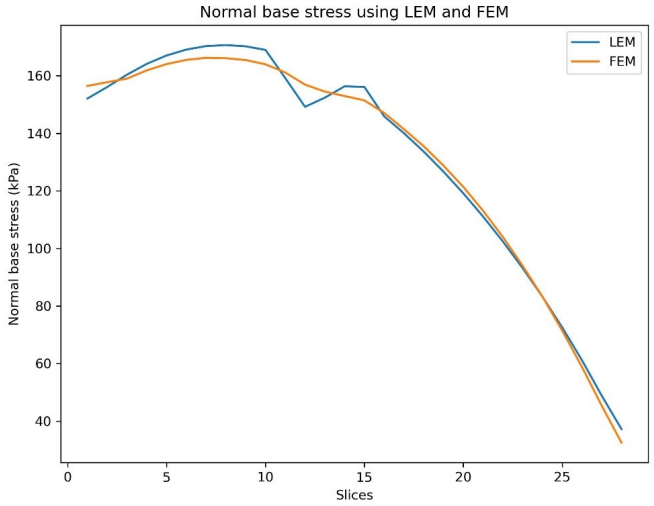

Figure 16. Base stress distributions plot of 28 slices using LEM and stress-based FEM.

3.1.2. Factor of Safety (FOS)

The LEM assumed that the FOS is the same for all the slices, which is not realistic, whereas stress-based FEM captures all the local factors of safety of each slice assuming the initial in situ stress distribution, as illustrated by the plot in Figure 17. Therefore, stress-based FEM is suitable for small-scale slope stability to capture the local FOS within the slope considering true stress–strain distribution.

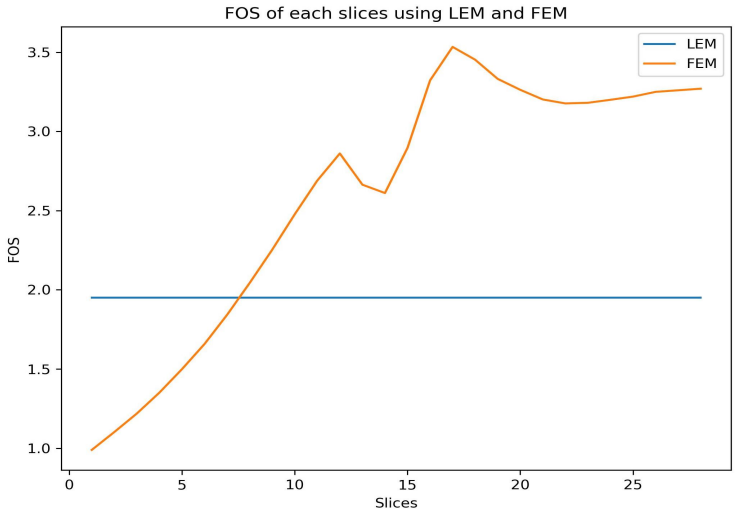

Figure 17. FOS using LEM and stress-based FEM for 28 slices.

3.2. Transient State

The unsteady seepage flow path due to changes in water level in the reservoirs leads to internal erosion and piping issues. The drawing down of the water level during the flushing of the reservoir is a critical task, as the drawn rate directly affects the sliding stability of the slope [7]. The quick reduction of water load and the change in pore–water pressure inside the earth-fill dam, depending upon the soil parameters, needs to be assessed for safe regulation of flushing without any instability of the slope. The evaluation of FOS considering different load cases is necessary to ensure the stability of the dam.

The coupled model of SEEP/W with SLOPE/W for LEM and stress-based FEM with SEEP/W and SIGMA/W for FEM were modeled to evaluate the FOS for different load cases. The unsteady seepage flow behaviors at different draw-down rates were evaluated by adopting the as-built design of the dam. The sensitivity analysis was carried out through the establishment of two cases, i.e., changing the permeability of the upstream dam shell and application of highly permeable horizontal filter material. The time-dependent FOS using LEM and stress-based FEM as well as nonlinear behaviors analysis using stress-based FEM with Mohr–Coulomb criteria were evaluated in the case of RDD, considering the case study of 8 h to identify the plastic zone regarding sliding stability analysis.

The time-dependent critical FOS using LEM adopting the Morgenstern–Price method and stress-based FEM were carried out for linear draw-down of 8 h, 20 h, 40 h, 60 h, and 80 h, as plotted in Figure 18. The different draw-down rates were established to identify the safe draw-down rate regarding the slope stability, as per the guidelines of the US Army Corps of Engineers [33].

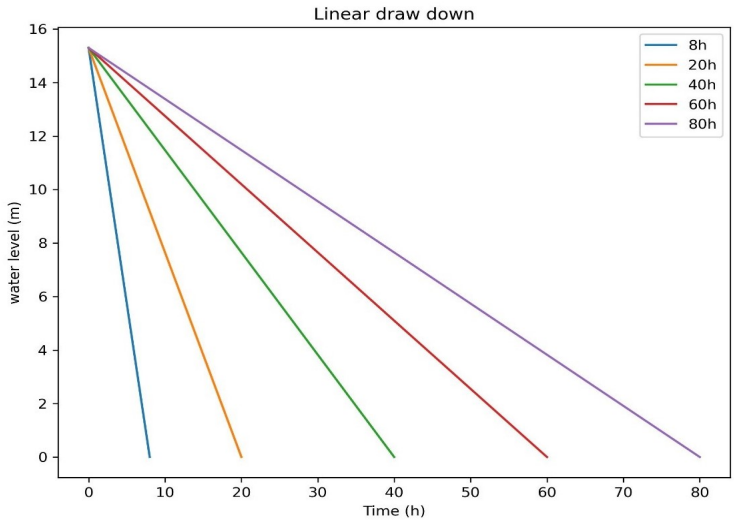

Figure 18. Linear draw-down water level.

3.2.1. Nonlinear Behavior Analysis

The stress–strain-based FEM coupled with SEEP/W and SIGMA/W was used to capture the nonlinear behaviors adapting Mohr–Coulomb failure criteria. The variation of time-dependent loads due to changes in water level during the draw-down shows the nonlinear behaviors, in relationship with the stress–strain distribution of the soil mass. To identify plastic zones due to the nonlinear behaviors of the soil mass, the adopted three different cases (i.e., as-built design, change in dam shell permeability, and application of horizontal filter materials) were carried out considering the case study of 8 h of RDD.

The nonlinear behavior mesh in a plastic state has been shaded with a yellow region as represented in Figures 19–21, indicating an unstable zone at the upstream side of the dam during the 8 h of draw-down with a rate of 1.91 m/h in all the cases. The model exhibits the maximum chances of movement of boulder rip-rap at the upstream side of the dam during the RDD. The results replicate the case of instability of the boulder rip-rap at the upstream side of the dam after 8 h of draw-down, which can be visualized through Figure 2.

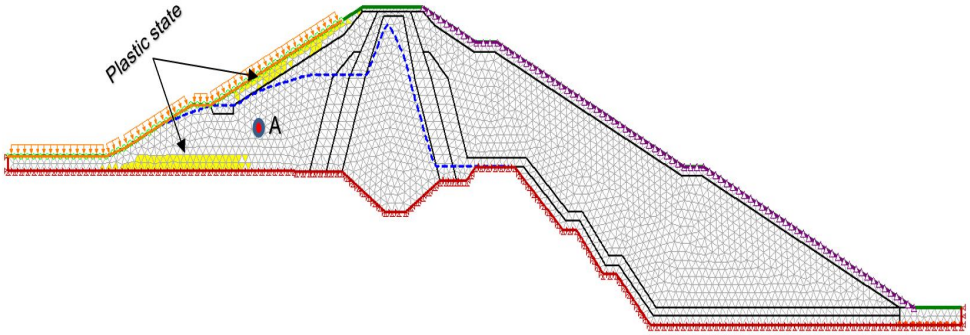

Figure 19. At 8 h with a draw-down rate of 1.91 m/h—upstream dam shell ($k_w = 1 \times 10^{-4}$ m/s).

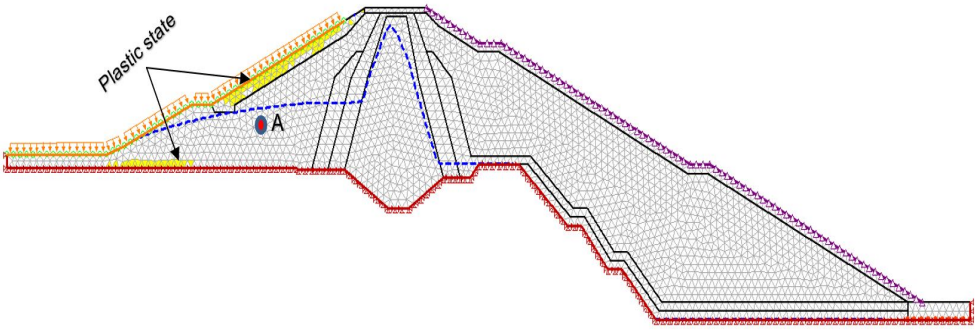

Figure 20. At 8 h with a draw-down rate of 1.91 m/h—upstream dam shell ($k_w = 8 \times 10^{-4}$ m/s).

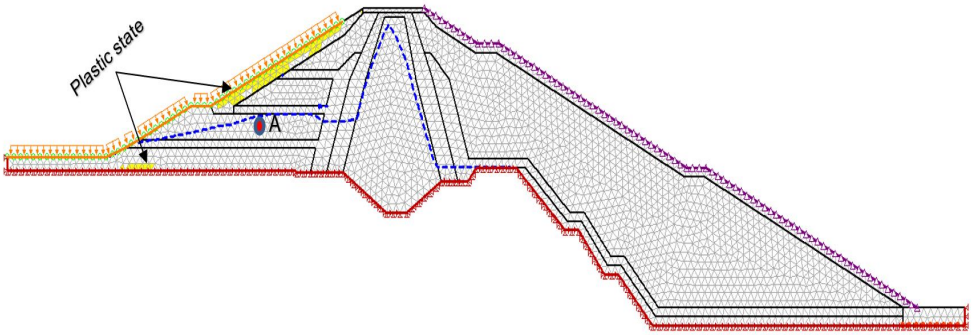

Figure 21. At 8 h with a draw-down rate of 1.91 m/h—three-layer horizontal filters (cross-section length = 33 m, 15 m, 8.5 m and height = 1 m with $k_w = 1 \times 10^{-2}$ m/s).

3.2.2. Pressure and Seepage Discharge Variation

The excess pore water pressure variation inside the dam highly dominates the FOS, as it reduces the resisting shear force [3,4]. Upstream dam materials should safely release the seepage discharge from the dam during the draw-down of water level, reducing the excess pore water pressure inside the dam. Therefore, three cases were established to evaluate the change in pressure and discharge at location A, as shown in Figures 19–21. The result illustrates that less excess pore water pressure was achieved inside the dam with increased permeability at the upstream dam shell, as it quickly releases the pore water pressure from the dam. The evolution of pore water pressure inside the dam for different cases of RDD has been plotted in Figure 22.

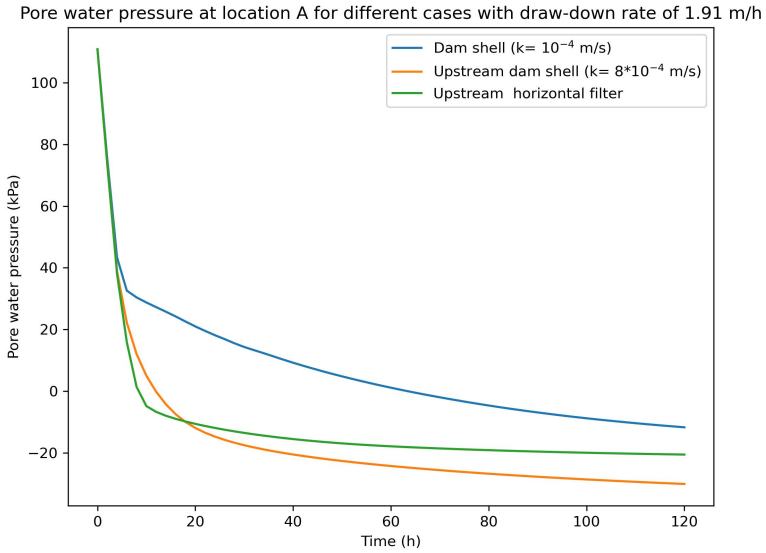

Figure 22. Pore water pressure at location A in Figures 19–21 with a draw-down rate of 1.91 m/h

The influence of change in permeability on seepage discharge and reduction of pore water pressure at location A was evaluated at 8 h. The obtained results of Table 6 illustrate that the higher permeability increases the seepage discharge and reduces the excess pore water pressure inside the dam, which can be clearly visualized through Figures 19–21.

Table 6. Seepage discharge at location A in Figures 19–21 with a draw-down rate of 1.91 m/h.

Upstream side of the dam at location A with a draw-down rate 1.91 m/h after 8 h	
Hydraulic conductivity (k_w) m/s	**Seepage discharge** $(m^3/s/m^2)$
1×10^{-4}	2.81×10^{-5}
8×10^{-4}	8.86×10^{-5}
Three-layers horizontal filter $= 1 \times 10^{-2}$ conductivity at location A is 1×10^{-4}	3.96×10^{-5}

3.2.3. Time-Dependent FOS and Pore Water Pressure Using LEM

The time-dependent FOS and pressure variation charts at location A were produced using LEM and stress-based FEM. LEM plots were only presented due to the similarity of the results. The resulting charts, as shown in Figures 23–25, clearly indicate that the FOS increases with the decreased draw-down rates. The decreased draw-down rate helps to reduce the excess pore water pressure inside the dam increasing resisting shear force, ultimately increasing the FOS against sliding. The plotted charts of time-dependent pore water pressure inside the dam at location A clearly indicate the evolution of pressure and its significant impact on FOS. The significant change in FOS was achieved through the sensitivity analysis considering two cases (i.e., increase in permeability of upstream dam shell and application of three layers of high permeable horizontal filter materials), which has shown a quick release of pore water pressure from the dam, which has a huge influence in increasing FOS during the draw-down.

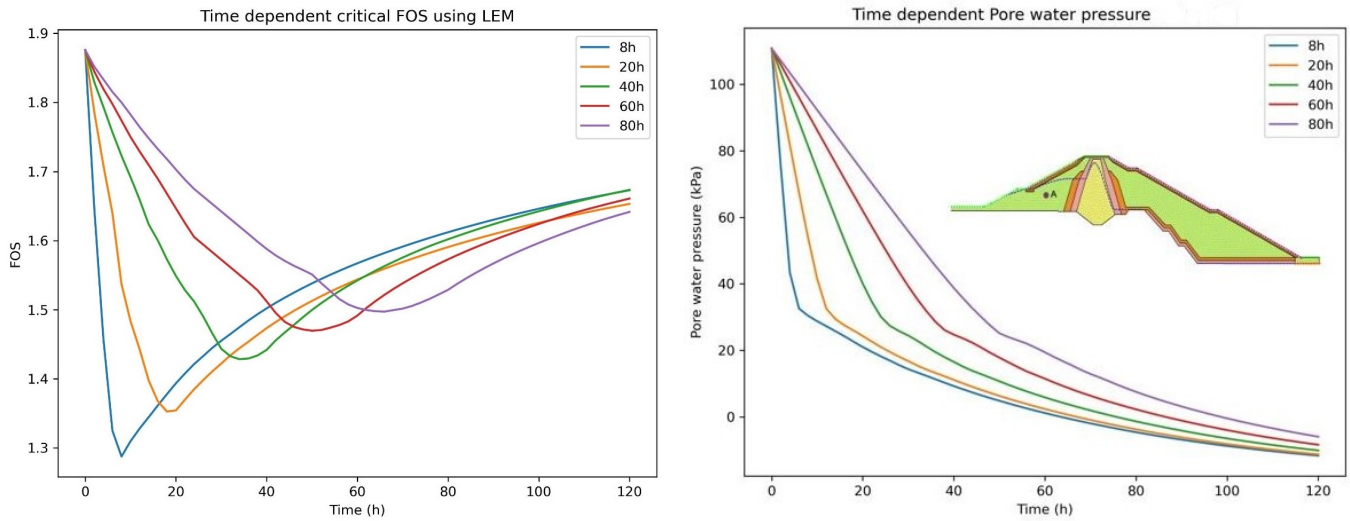

Figure 23. Left represents FOS and right illustrates pore water pressure at location A for different draw-down rates using LEM (Upstream dam shell ($k_w = 10^{-4}$ m/s)).

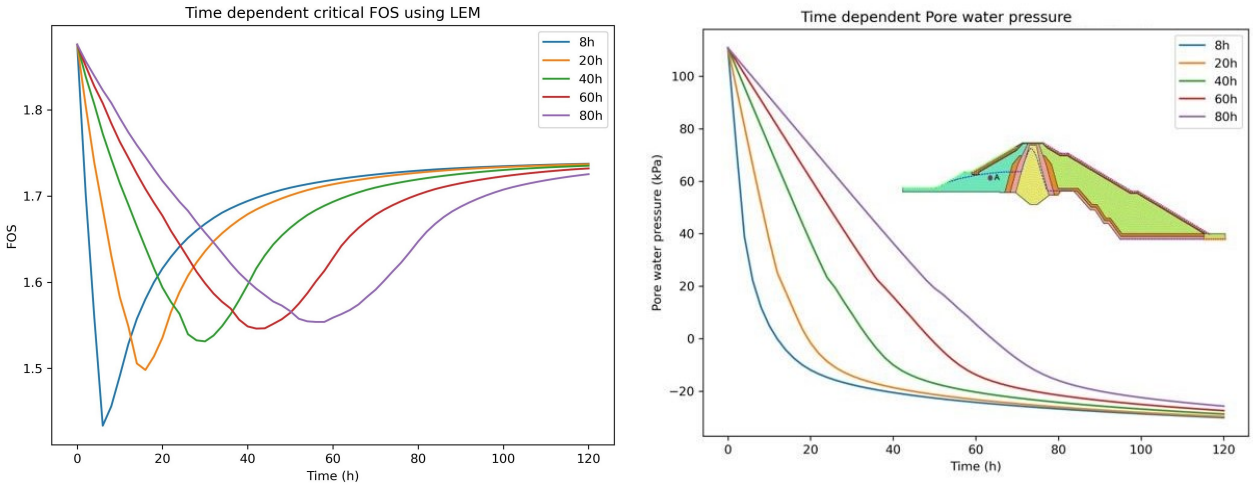

Figure 24. Left represents FOS and right illustrates pore water pressure at location A for different draw-down rates using LEM (Upstream dam shell ($k_w = 8 \times 10^{-4}$ m/s)).

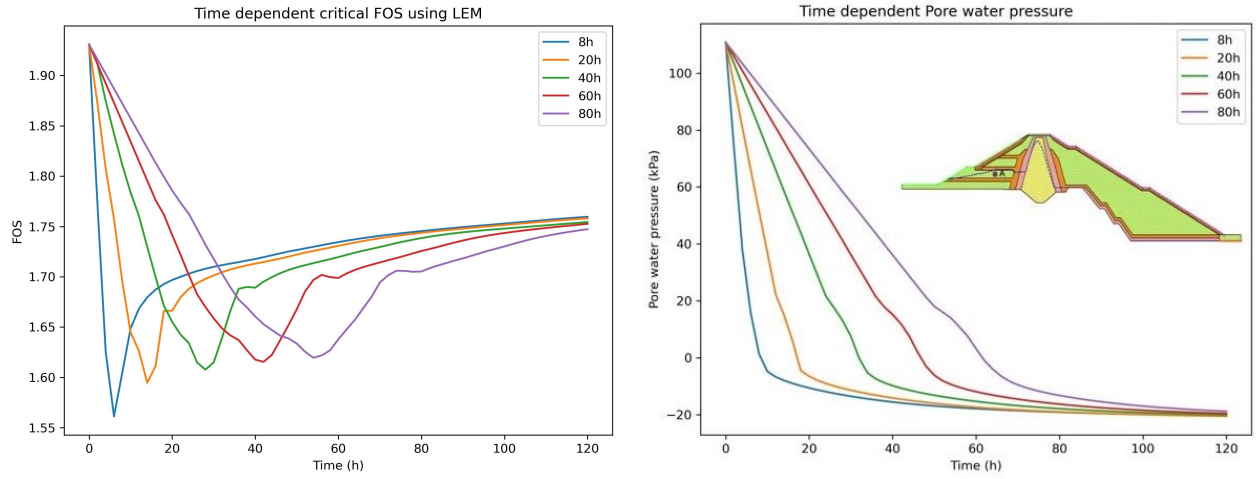

Figure 25. Left represents FOS and right illustrates pore water pressure at location A for different draw-down rates using LEM (Upstream three horizontal filter layers ($k_w = 1 \times 10^{-2}$ m/s)).

4. Discussion

4.1. Steady-State Conditions

The long-term stability assessment was carried out considering the steady state of the as-built design dam to ensure stability in steady-state conditions. Overall critical FOS, base-slice stress distribution, and local slice FOS were evaluated and compared using different coupled models of LEM and stress-based FEM.

A safe overall critical FOS of 1.92 and 1.89 were obtained through LEM and stress-based FEM, as plotted in Figures 14 and 15, which satisfied the minimum required factors of safety for rock-fill dams as per the guidelines of the US Army Corps of Engineers, summarized in Table 7. The stress distribution plot of Figure 16 at the base of each slice shows more or less the same distribution on each slice considering the equal radius of the slip circle using LEM and stress-based FEM; as a result, overall critical FOS was found to be more or less similar. Figure 17 illustrate the capabilities of stress-based FEM over LEM. Local FOS was also able to capture by stress-based FEM, as the LEM depends on a predefined slip circle, which results in constant FOS for all the slices, whereas the stress-based FEM is based on the stress–strain distribution defined by the mechanical properties of soil mass.

Table 7. Minimum required factors of safety: new earth and rock-fill dams, US Army Corps of Engineers [33].

Analysis Condition [1]	Required Minimum Factor of Safety	Slope
End-of-Construction (including staged construction) [2]	1.3	Upstream and Downstream
Long-term (Steady seepage, maximum storage pool, spillway crest or top of gates)	1.5	Upstream and Downstream
Maximum surcharge pool [3]	1.4	Downstream
Rapid Draw Down	1.1–1.3 [4,5]	Upstream

[1] For earthquake loading, see ER 1110-2-1806 [33] for guidance. An Engineer Circular, "Dynamic Analysis of Embankment Dams", is still in preparation. [2] For embankments over 50 feet high on soft foundations and for embankments that will be subjected to pool loading during construction, a higher minimum end-of-construction factor of safety may be appropriate. [3] Pool thrust from maximum surcharge level. Pore pressures are usually taken as those developed under steady-state seepage at maximum storage pool. However, for pervious foundations with no positive cutoff steady-state seepage may develop under the maximum surcharge pool. [4] Factor of safety (FS) to be used with the improved method of analysis described in Appendix G of US Army Corps of Engineers [33] [5] FS = 1.1 applies to draw-down from the maximum surcharge pool; FS = 1.3 applies to draw-down from the maximum storage pool. For dams used in pump storage schemes or similar applications where RDD is a routine operating condition, higher factors of safety, e.g., 1.4–1.5, are appropriate. If the consequences of an upstream failure are great, such as blockage of the outlet works resulting in a potential catastrophic failure, higher factors of safety should be considered.

4.2. Transient State

The sliding slope instability due to variation of loads in the dam, induced as a result of a change in reservoir water levels, was tested with different draw-down rates. The sliding stability of the slope was evaluated by defining the critical FOS using LEM, stress-based FEM, and nonlinear analysis using stress-based FEM in the case of RDD. Evaluation of time-dependent pore water pressure and seepage discharge was carried out to observe the impact of the change in material properties and water level regulation.

The overall critical FOS using the LEM and stress-based FEM was found to be more or less similar, though the resulting values of FOS might differ due to various reasons. LEM relies on the equilibrium equations and depends upon the predefined failure surface, which does not consider the actual condition of the nature, i.e., the behavior of the soil parameter [8]. On the other hand, the true complex behavior of the soil is hard to determine

and might not be truly represented, which results in uncertainties in the analysis for stress-based FEM.

In the case of as-built design, the obtained summary Table 8 based on the results from Figures 23–25 has shown that the minimum critical FOS of 1.28 and 1.27 during the RDD with a rate of 1.91 m/h for 8 h was identified to be unsafe, as per the US Army Corps of Engineers. The FOS obtained from LEM and stress-based FEM were found to be less than 1.3. The US Army Corps of Engineers guidelines (Table 7) state that "[5]FS = 1.3 applies to draw-down from the maximum storage pool" to be safe against sliding. The allowable draw-down rate of 0.76 m/h for 20 h was found to be safe as FOS reaches 1.35, which satisfies the minimum critical FOS criteria. The large pore water pressure gradient should be avoided to protect against internal erosion and cracks [18].

The additional two test cases (i.e., increased permeability of upstream dam shell and application of three layers of highly permeable horizontal filter materials) for parameter sensitivity analysis have shown adequate FOS results, as illustrated by Table 8 for all draw-down rates. The results have shown that the FOS is highly dominated by the permeability of the material and draw-down rate in the case of reservoir draw-down. The critical minimum FOS values were found to be more than 1.3 in all the draw-down rates for both cases, as represented by Table 8. Figures 19–21 show how the phreatic line changes inside the upstream side of the dam with the influence of change in seepage discharge and pore water pressure, as estimated and plotted in Table 6 and Figure 22. This indicates FOS is highly dominated by the upstream dam shell permeability. Therefore, a safe allowable draw-down rate and quick release of the excess pore water pressure are the two crucial things that govern the FOS at the time of RDD. The draw-down rate should be maintained by using a critical FOS value above 1.3, as per the guidelines set by the US Army Corps of Engineers [33].

Table 8. Overall critical minimum FOS using LEM and stress-based FEM.

Overall Minimum FOS							
Draw-Down	**Draw-Down Rate**	**Dam Shell ($k_w = 10^{-4}$)**		**Dam Shell ($k_w = 8 \times 10^{-4}$)**		**Upstream Horizontal Filter**	
		Using LEM	**Using FEM**	**Using LEM**	**Using FEM**	**Using LEM**	**Using FEM**
8 h	1.91 m/h	1.28	1.27	1.43	1.41	1.56	1.54
20 h	0.76 m/h	1.35	1.33	1.49	1.47	1.59	1.57
40 h	0.38 m/h	1.42	1.38	1.53	1.51	1.60	1.58
60 h	0.25 m/h	1.46	1.42	1.54	1.52	1.61	1.59
80 h	0.19 m/h	1.49	1.44	1.55	1.53	1.62	1.60

However, nonlinear analysis with stress-based FEM has shown instability of slope in the rip-rap zone and at the toe of the dam for all three cases, with a draw-down rate of 1.91 m/h for 8 h, as represented in Figures 19–21. The plastic zone has been seen after 8 h of RDD in all three cases. Therefore, it was found that the instability of the slope is not fully defined by the critical slip based on the minimum overall FOS. The localized regions or elements within the slope that are experiencing plastic deformation or yielding might go beyond the theory of traditional equilibrium method, as represented in Figures 19–21.

5. Conclusions

Coupled model comparisons of LEM and stress-based FEM were used to investigate the sliding slope stability under steady and transient states. The FOS and nonlinear behavior analyses were carried out to ensure the stability of the slope during draw-down. The following conclusions can be specifically drawn from the present study:

1. The long-term steady-state analysis has resulted in a similar FOS of 1.92 with LEM and 1.89 with stress-based FEM. The identical slip circles resulted in similar base stress distribution, using both models. As a result, similar FOS values were obtained.
2. Considering the as-built design dam with 8 h of RDD, a critical FOS of less than 1.3 was obtained. It was classified as unsafe according to the guidelines. A safe allowable

draw-down rate of 0.76 m/h for 20 h was identified to reach the minimum critical FOS criteria.

3. The sensitivity analyses' test results have shown that the FOS values are significantly dominated by upstream dam shell permeability and draw-down rates. The slow draw-down rates and quick release of excess pore water pressure are important to ensure safe sliding stability. The additional test case with a horizontal filter provided adequate FOS for all draw-down rates.
4. The coupled stress-based FEM for the nonlinear behavior analysis was carried out in the case of 8 h of RDD. The local plastic deformation in the upstream slope and at the toe of the dam has been observed, which was not seen in the equilibrium method.
5. To ensure dam safety during RDD, the allowable draw-down rate should be evaluated. The appropriate permeability of the dam shell and horizontal filters must be considered during the design and construction phase.

Author Contributions: B.R.P.: writing and editing; H.K.: review and editing; G.Z.: review and editing. All authors have read and agreed to the published version of the manuscript.

Funding: Open Access Funding by the Graz University of Technology.

Data Availability Statement: Some data are retrieved from open-source platforms, while other data are not publicly available due to data confidentiality.

Conflicts of Interest: The authors declare no conflict of interest.

References

1. Sjödahl, P.; Dahlin, T.; Johansson, S. Using resistivity measurements for dam safety evaluation at Enemossen tailings dam in southern Sweden. *Environ. Geol.* **2005**, *49*, 267–273. [CrossRef]
2. Andersen, G.R.; Chouinard, L.E.; Bouvier, C.; Back, W.E. Ranking procedure on maintenance tasks for monitoring of embankment dams. *J. Geotech. Geoenviron. Eng.* **1999**, *125*, 247–259. [CrossRef]
3. Al-Janabi, A.M.S.; Ghazali, A.H.; Ghazaw, Y.M.; Afan, H.A.; Al-Ansari, N.; Yaseen, Z.M. Experimental and numerical analysis for earth-fill dam seepage. *Sustainability* **2020**, *12*, 2490. [CrossRef]
4. Sun, G.; Yang, Y.; Jiang, W.; Zheng, H. Effects of an increase in reservoir drawdown rate on bank slope stability: A case study at the Three Gorges Reservoir, China. *Eng. Geol.* **2017**, *221*, 61–69. [CrossRef]
5. Alonso, E.E.; Pinyol, N.M. Numerical analysis of rapid drawdown: Applications in real cases. *Water Sci. Eng.* **2016**, *9*, 175–182. [CrossRef]
6. Utepov, Y.; Lechowicz, Z.; Zhussupbekov, A.; Skutnik, Z.; Aldungarova, A.; Mkilima, T. The influence of material characteristics on dam stability under rapid drawdown conditions. *Arch. Civ. Eng.* **2022**, *38*, 539–553.
7. Pinyol, N.M.; Alonso, E.E.; Olivella, S. Rapid drawdown in slopes and embankments. *Water Resour. Res.* **2008**, *44*, W00D03. [CrossRef]
8. Duncan, J.M. State of the art: Limit equilibrium and finite-element analysis of slopes. *J. Geotech. Eng.* **1996**, *122*, 577–596. [CrossRef]
9. Cheng, Y.M.; Yip, C. Three-dimensional asymmetrical slope stability analysis extension of Bishop's, Janbu's, and Morgenstern—Price's techniques. *J. Geotech. Geoenviron. Eng.* **2007**, *133*, 1544–1555. [CrossRef]
10. Lane, P.; Griffiths, D. Assessment of stability of slopes under drawdown conditions. *J. Geotech. Geoenviron. Eng.* **2000**, *126*, 443–450. [CrossRef]
11. Oo, H.Z.; Ai, L.Z.; Qiu, Z. Numerical analysis of river bank slope stability during rapid drawdown of water level. *Study Civ. Eng. Arch.* **2013**, *2*, 98–103.
12. Hammouri, N.A.; Malkawi, A.I.H.; Yamin, M.M. Stability analysis of slopes using the finite element method and limiting equilibrium approach. *Bull. Eng. Geol. Environ.* **2008**, *67*, 471–478. [CrossRef]
13. Azadi, A.; Esmatkhah Irani, A.; Azarafza, M.; Hajialilue Bonab, M.; Sarand, F.B.; Derakhshani, R. Coupled numerical and analytical stability analysis charts for an earth-fill dam under rapid drawdown conditions. *Appl. Sci.* **2022**, *12*, 4550. [CrossRef]
14. Utepov, Y.B.; Aldungarova, A.K.; Mkilima, T.; Pidal, I.M.; Tulebekova, A.S.; Zharassov, S.Z.; Abisheva, A.K. Dynamics of Embankment Slope Stability under Combination of Operating Water Levels and Drawdown Conditions. *Infrastructures* **2022**, *7*, 65. [CrossRef]
15. Srivastava, A.; Babu, G.S.; Haldar, S. Influence of spatial variability of permeability property on steady state seepage flow and slope stability analysis. *Eng. Geol.* **2010**, *110*, 93–101. [CrossRef]
16. Gottardi, G.; Gragnano, C.G.; Rocchi, I.; Bittelli, M. Assessing river embankment stability under transient seepage conditions. *Procedia Eng.* **2016**, *158*, 350–355. [CrossRef]

17. Bhaskar, P.; Puppala, A.J.; Boluk, B. Influence of unsaturated hydraulic properties on transient seepage and stability analysis of an earthen dam. *Int. J. Geomech.* **2022**, *22*, 04022105. [CrossRef]
18. Li, Z.; Ye, W.; Marence, M.; Bricker, J.D. Unsteady seepage behavior of an earthfill dam during drought-flood cycles. *Geosciences* **2018**, *9*, 17. [CrossRef]
19. Alonso Pérez de Agreda, E.; Pinyol Puigmartí, N.M. Slope stability under rapid drawdown conditions. In Proceedings of the First Italian Workshop on Landslides, Landslides, Napoli, 8–10 June 2009; pp. 11–27. Available online: https://upcommons.upc.edu/bitstream/handle/2117/11200/01_IWL2009_Alonso-Pinyol.pdf?sequence=1 (accessed on 30 October 2023).
20. Nepal-Electricity-Authority (NEA). 9th Issue, Generation Operation and Maintenance Business. Technical Report. 2013. Available online: https://www.nea.org.np/admin/assets/uploads/supportive_docs/GenerationOM9thIssue.pdf (accessed on 30 October 2023).
21. Giri, S.; Omer, A.; Mool, P.; Kitamura, Y. Morphological modelling of sediment-induced problems at a cascade system of hydropower projects in hilly region of Nepal. In *Sustainable and Safe Dams around the World/Un Monde de Barrages Durables et Sécuritaires*; CRC Press: Boca Raton, FL, USA, 2019; pp. 1306–1317. Available online: https://www.taylorfrancis.com/chapters/edit/10.1201/9780429319778-113/morphological-modelling-sediment-induced-problems-cascade-system-hydropower-projects-hilly-region-nepal-giri-omer-mool-kitamura (accessed on 30 October 2023).
22. Army Engineer Waterways Experiment Station Vicksburg MS. The Unified Soil Classification System. Appendix A. Characteristics of Soil Groups Pertaining to Embankments and Foundations. Appendix B. Characteristics of Soil Groups Pertaining to Roads and Airfields. 1967. Available online: https://apps.dtic.mil/sti/pdfs/ADA026473.pdf (accessed on 30 October 2023).
23. Zhai, Q.; Rahardjo, H. Quantification of uncertainties in soil–water characteristic curve associated with fitting parameters. *Eng. Geol.* **2013**, *163*, 144–152. [CrossRef]
24. Leong, E.C.; Rahardjo, H. Review of soil-water characteristic curve equations. *J. Geotech. Geoenviron. Eng.* **1997**, *123*, 1106–1117. [CrossRef]
25. Khire, M.V.; Benson, C.H.; Bosscher, P.J. Capillary barriers: Design variables and water balance. *J. Geotech. Geoenviron. Eng.* **2000**, *126*, 695–708. [CrossRef]
26. Van Genuchten, M.T. A closed-form equation for predicting the hydraulic conductivity of unsaturated soils. *Soil Sci. Soc. Am. J.* **1980**, *44*, 892–898. [CrossRef]
27. Ameratunga, J.; Sivakugan, N.; Das, B.M. *Correlations of Soil and Rock Properties in Geotechnical Engineering*; Springer: New Delhi, India, 2016. [CrossRef]
28. Bowles, J.E. Physical and Geotechnical Properties of Soils. 1979. Available online: https://trid.trb.org/view/82144 (accessed on 30 October 2023).
29. AASTHO. *LRFD Bridge Design Specifications (SI)*; American Association of State Highway and Transportation Officials: Washington, DC, USA, 2007; p. 1037. Available online: https://s36d44bae16611495.jimcontent.com/download/version/1650043778/module/11581789993/name/AASHTO_LRFD_Bridge_Design_Specifications.pdf (accessed on 30 October 2023).
30. Verruijt, A. *Soil Mechanics/Arnold Verruijt*; Delft University of Technology: Delft, The Netherlands, 2001. Available online: https://ocw.tudelft.nl/wp-content/uploads/SoilMechBook.pdf (accessed on 30 October 2023).
31. Smith, I. *Smith's Elements of Soil Mechanics*; John Wiley & Sons: Hoboken, NJ, USA, 2021. Available online: https://ds.amu.edu.et/xmlui/bitstream/handle/123456789/9472/%5BG._N._Smith_G.N._Smith%5D_Elements_of_Soil_Mechanic%28BookFi.org%29.pdf?sequence=1&isAllowed=y (accessed on 30 October 2023).
32. Geostudio. Stability Modeling with GeoStudio. 2023. Available online: https://www.geoslope.com/learning/support-resources#dnn_BooksHeaderPane (accessed on 30 October 2023).
33. U.S. Army Corps of Engineers. Slope Stability, Engineering Manual. 2023. Available online: https://www.publications.usace.army.mil/Portals/76/Publications/EngineerManuals/EM_1110-2-1902.pdf (accessed on 30 October 2023).

Disclaimer/Publisher's Note: The statements, opinions and data contained in all publications are solely those of the individual author(s) and contributor(s) and not of MDPI and/or the editor(s). MDPI and/or the editor(s) disclaim responsibility for any injury to people or property resulting from any ideas, methods, instructions or products referred to in the content.